

Vibrational mode and collision energy effects on reaction of H_2CO^+ with C_2D_4

Jianbo Liu, Brian Van Devener, and Scott L. Anderson^{a)}
Department of Chemistry, University of Utah, Salt Lake City, Utah 84112

(Received 16 August 2004; accepted 1 October 2004)

We report the effects of collision energy (E_{col}) and five different H_2CO^+ vibrational modes on the reaction of H_2CO^+ with C_2D_4 over the center-of-mass E_{col} range from 0.1 to 2.1 eV. Properties of various complexes and transition states were also examined computationally. Seven product channels are observed. Charge transfer (CT) has the largest cross section over the entire energy range, substantially exceeding the hard sphere cross section at high energies. Competing with CT are six channels involving transfer of one or more hydrogen atoms or protons and one involving formation of propanal, followed by hydrogen elimination. Despite the existence of multiple deep wells on the potential surface, all reactions go by direct mechanisms, except at the lowest collision energies, where short-lived complexes appear to be important. Statistical complex decay appears adequate to account for the product branching at low collision energies, however, even at the lowest energies, the vibrational effects are counter to statistical expectations. The pattern of E_{col} and vibrational mode effects provide insight into factors that control reaction and interchannel competition. © 2004 American Institute of Physics. [DOI: 10.1063/1.1822921]

I. INTRODUCTION

A common feature of ion-molecule reactions is the existence of intermediate complexes that can mediate reaction, particularly at low collision energies where the complex lifetime can be long.¹ Several types of complexes are possible. Nearly all ion-molecule systems have reactantlike electrostatic complexes. Such complexes can be important at low collision energy, mediating reorientation of reactants into more stable complexes or reactive geometries. Hydrogen-bonded complexes allow hydrogen or proton transfer, and may mediate rearrangement into other reactive geometries. When one or both reactants contain unsaturated bonds, covalently bound complexes may mediate complicated reactions with multiple bonds broken and formed. The H_2CO^+ + C_2H_4 system has all three types of complexes, mediating seven product channels. To unravel such complicated reaction dynamics, a combination of detailed experiments and theory is needed.

Here we report a vibrationally mode-selective differential scattering study. Integral cross sections and product velocity distributions were measured for reaction of mode-selectively excited H_2CO^+ with C_2D_4 over a wide range of collision energy (E_{col}). The E_{col} and vibrational state dependence of the cross sections gives information about interchannel competition and insight into the effects of energy, angular momentum, and different types of nuclear motion. When vibrational effects are mode dependent, rather than simple energy effects, the implication is that the critical point along the reaction coordinate is early enough that the initial vibrational mode information has not been scrambled. Product recoil velocity distributions provide complementary in-

formation regarding collision time scale, scattering mechanisms, degree of energy randomization, and exit channel interactions. Quantum chemistry calculations were used to find complexes and transition states on the reaction coordinate, then Rice-Ramsperger-Kassel-Marcus (RRKM) theory was used to estimate the statistical behavior expected for the system, for comparison with observation. Finally, direct dynamics and analytic potential classical trajectory calculations were used to probe issues relating to energy transfer and trajectory deflection in long-range collisions.

One interesting feature of the H_2CO^+ + C_2D_4 system is that there are three pairs of product channels differing only in which fragment carries the charge. The first pair is H_2CO^+ + C_2D_4 (charge transfer, CT) vs H_2CO^+ + C_2D_4 (nonreactive scattering, NR). The second pair is HCO^+ + $\text{C}_2\text{D}_4\text{H}$ (hydrogen transfer, HT) vs HCO^+ + $\text{C}_2\text{D}_4\text{H}^+$ (proton transfer, PT). The third pair is chemically identical to the first, but with H/D exchange: HDCO^+ + $\text{C}_2\text{D}_3\text{H}$ vs HDCO^+ + $\text{C}_2\text{D}_3\text{H}^+$. The E_{col} and vibrational state dependence of the branching within and between the product pairs provides insight into charge state coupling and decoupling during the course of collisions.

II. EXPERIMENTAL AND COMPUTATIONAL DETAILS

The guided ion beam tandem mass spectrometer used in this study has been described previously,²⁻⁵ along with the operation, calibration, and data analysis procedures. The H_2CO precursor was generated from paraformaldehyde (Aldrich 95%) mixed with anhydrous MgSO_4 (Merck) at 60 °C.⁶ The resulting H_2CO was carried into a pulsed molecular beam valve using a flow of helium at ~1 atm, giving a H_2CO concentration of ~5%.⁷ H_2CO^+ can be generated in selected vibrational states by resonance-enhanced multiphoton ionization through the $^1A_2(3p_x)$ Rydberg state.⁸ For this

^{a)} Author to whom correspondence should be addressed; Electronic mail: anderson@chem.utah.edu

study, H_2CO^+ was generated in its ground state or with one quantum in the following vibrational modes: ν_2^+ (CO stretch, 0.208 eV), ν_3^+ (CH_2 scissors, 0.143 eV), ν_4^+ (CH_2 out-of-plane bend, 0.114 eV), ν_5^+ (CH_2 asymmetric stretch, 0.337 eV), and ν_6^+ (CH_2 rock, 0.101 eV). The ions were generated inside a short radio frequency (rf) quadrupole ion guide which focused the ions through a pair of ion lenses into a quadrupole mass filter. Mass-selected ions were collected and collimated by a lens set equipped with variable apertures and an electrode pair used to time gate the ion pulse. The combination of controlled collection radius and time gating allows us to produce a mass-selected beam with narrow kinetic energy spread ($\Delta E \approx 0.1$ eV).

The mass-, vibrational state-, and kinetic energy-selected primary beam was injected into a system of eight-pole rf ion guides.⁹ In the first segment of the guide ions were passed through a 10 cm long scattering cell, containing C_2D_4 (Cambridge Isotope Lab, D_4 98%) at 4.0×10^{-5} Torr. Product ions and unreacted primary ions were collected by the ion guide, passed into a second, longer guide segment for time-of-flight (TOF) analysis, then mass analyzed and counted. Integral cross sections were calculated from the ratio of reactant and product ion intensities, and the calibrated target gas pressure-length product. TOF was used to measure the reactant ion beam velocity distribution (and thus the E_{col} distribution) at each nominal E_{col} and also to measure the product ion axial velocity distributions discussed below.

For each reactant state we cycled through the series of E_{col} values several times in order to minimize systematic error from drifting potentials, etc. As a check on reproducibility, we measured the cross sections for the ground state, both at the beginning and end of each complete experimental run. Finally, the entire set of experiments was repeated several times. Based on the reproducibility of the cross section measurements, we estimate that the relative error (e.g., uncertainty in comparing data for different vibrational states or

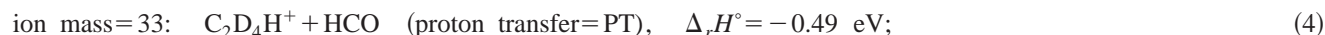
E_{col}) is less than 10%. The uncertainty in the absolute scale of the cross section is also estimated to be $\sim 10\%$, primarily resulting from uncertainties in target pressure and collection efficiency for slow product ions.

To map out the energetics of the reaction coordinates, electronic structure calculations were performed at the B3LYP/6-311++G** level of theory, using GAUSSIAN03.¹⁰ Geometries were optimized calculating the force constants at every point. The vibrational frequencies and zero-point energies were scaled by a factor of 0.9613 and 0.9804, respectively.¹¹ All transition states (TS) were verified to be first-order saddle points by frequency calculations. RRKM calculations were done with the program of Zhu and Hase,¹² using its direct state count option, and frequencies and energetics from the B3LYP/6-311++G** calculations. Direct dynamics trajectories were calculated at the MP2/6-31G* level of theory, using the updating Hessian trajectory integrator built into GAUSSIAN03,¹⁰ with initial conditions generated by the VENUS program of Hase *et al.*¹³ Trajectories evaluating the role of the long-range potential on the range of impact parameters leading to CT were integrated using a homemade classical trajectory program and analytic electrostatic potentials. The ion-induced dipole potential was used for the $\text{H}_2\text{CO}^+ + \text{C}_2\text{D}_4$ charge state, while for $\text{H}_2\text{CO} + \text{C}_2\text{D}_4^+$ the ion-dipole potential was used. In the latter case a potential corresponding to the average dipole orientation was used for long range and the possibility for dipole orientation locking at some specified distance was also included.

III. RESULTS AND ANALYSIS

A. Integral cross sections

The $\text{H}_2\text{CO}^+ + \text{C}_2\text{D}_4$ isotope combination was used to look for hydrogen scrambling during reactions. The following product channels are observed, where energetics (298 K) are taken from Lias and co-workers:^{14,15}



Note that the ‘‘H/D exchange’’ and ‘‘rearrangement CT’’ channels are just the two charge states of the $(\text{HDCO} + \text{C}_2\text{D}_3\text{H})^+$ product pair, and coincidentally also have the same product ion mass. Because they cannot be distinguished, we will refer to the sum of these two channels as H_Ex.

The integral cross sections for reaction of ground state H_2CO^+ with C_2D_4 are shown in Fig. 1 over the center-of-mass (c.m.) E_{col} range from 0.1 to 2.1 eV. Also shown are the experimental total cross section (σ_{total} =sum of individual cross section) and an estimate of the collision cross section ($\sigma_{\text{collision}}$), taken as greater of the capture cross section

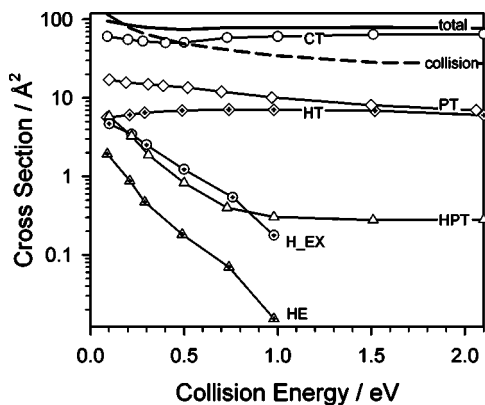


FIG. 1. Cross sections for the reaction of ground state H_2CO^+ with C_2D_4 . Also shown are the total reaction cross section and the estimated collision cross section.

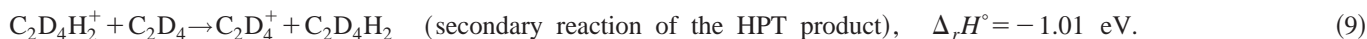
(σ_{capture}) and the hard sphere cross section ($\sigma_{\text{hardsphere}}$). $\sigma_{\text{hardsphere}}$ was calculated from the orientation-averaged contact radius of H_2CO^+ and C_2D_4 , assuming covalent radii for each atom, and exceeds σ_{capture} for $E_{\text{col}} > \sim 1.5$ eV.

The dominant channel at all collision energies is CT. The CT channel is suppressed by collision energy at low E_{col} , approaches a minimum at $E_{\text{col}} = 0.4$ eV, and then rebounds, eventually becoming energy-independent at high E_{col} . The

CT efficiency ($= \sigma_{\text{CT}} / \sigma_{\text{collision}}$) increases from 50% at low E_{col} to 230% at high E_{col} . The fact that σ_{CT} exceeds $\sigma_{\text{collision}}$ for $E_{\text{col}} \geq 0.5$ eV, indicates that CT can take place at large interreactant separations. As a consequence, σ_{total} exceeds $\sigma_{\text{collision}}$ except at the lowest collision energy.

The PT cross section declines with E_{col} however the PT efficiency ($= \sigma_{\text{PT}} / \sigma_{\text{collision}}$) increases from 15%–20% at low E_{col} to a E_{col} -independent 27% at high E_{col} . For the HT channel, both the cross section and reaction efficiency increase with E_{col} , with efficiency approaching 22% at the highest E_{col} . Note that the HT signal (HCO^+) may have a contribution from collision-induced dissociation (CID) of H_2CO^+ , however, several pieces of evidence suggest that the CID contribution is negligible (see below). The HPT channel is strongly suppressed by E_{col} at low energies and becomes energy-independent ($\sim 1\%$) at high energies. The cross sections for H_EX and HE have E_{col} dependence different from the above channels. Both are strongly suppressed by E_{col} declining to near-zero cross section (efficiency $< 0.3\%$) at E_{col} above 1.0 eV.

An issue for this system is that the C_2D_4^+ , $\text{C}_2\text{D}_4\text{H}^+$, and $\text{C}_2\text{D}_4\text{H}_2^+$ products have low velocities in the lab frame (see below), and are likely to undergo secondary reactions with the C_2D_4 in the scattering cell. Significant signal is seen for masses corresponding to the following secondary reactions:^{14–16}



The integral cross sections reported in Fig. 1 were corrected for these secondary reactions by taking measurements at several C_2D_4 pressures ranging from 1.0×10^{-4} to 4.0×10^{-5} Torr, then extrapolating to zero C_2D_4 pressure. In addition, the cross sections have been corrected for contributions from the isotopic C_2D_4 contaminants: $^{13}\text{CD}_2\text{CD}_2$ and $\text{C}_2\text{D}_3\text{H}$, both having $\sim 2\%$ concentration in the C_2D_4 .

There are also a number of mass overlaps that potentially complicate assignment of some product ion masses to particular reactions. The CT product mass (C_2D_4^+) could have contributions from H_2COD^+ (hydrogen abstraction, HA) and from D_2CO^+ (double H/D exchange). HA is endoergic by 0.22 eV, thus could only contribute at $E_{\text{col}} > 0.22$ eV. Even at high energies, however, competition with facile exoergic channels (CT,PT,HT) makes it quite unlikely that this endoergic channel could account for more than a few percent of the huge CT cross section. Furthermore, experience suggests^{17,18} that HA should give strongly forward-peaked product ions at high E_{col} , whereas the CT product ions are strongly backward peaked, as expected (see below). Double H/D exchange is certainly possible, but unlikely to

be significant, given that the cross section for single H/D exchange (H_EX) is small. Multiple H/D exchange could also conceivably generate d_2 - and d_3 - H_2COH^+ contributions to the PT and HPT signals, respectively. Again, multiple H/D exchange appears unlikely to be efficient enough for such contributions to be significant, particularly for the large PT cross section.

B. Computational results

The computational results for $\text{H}_2\text{CO}^+ + \text{C}_2\text{H}_4$ are summarized in Fig. 2 and Table I. Energetics are reported for all H species to allow comparison with the literature, however, the calculated energy differences for the appropriate deuterated species are generally small and always < 0.1 eV, i.e., within the computational uncertainty. The B3LYP results are in reasonable agreement with experiment, the exception being that the HE reaction is calculated to be less exoergic by 0.57 eV. In Fig. 2, the energetics for products are experimental, and those for complexes and TSSs are experimental, where available, and B3LYP/6-311++G** otherwise.

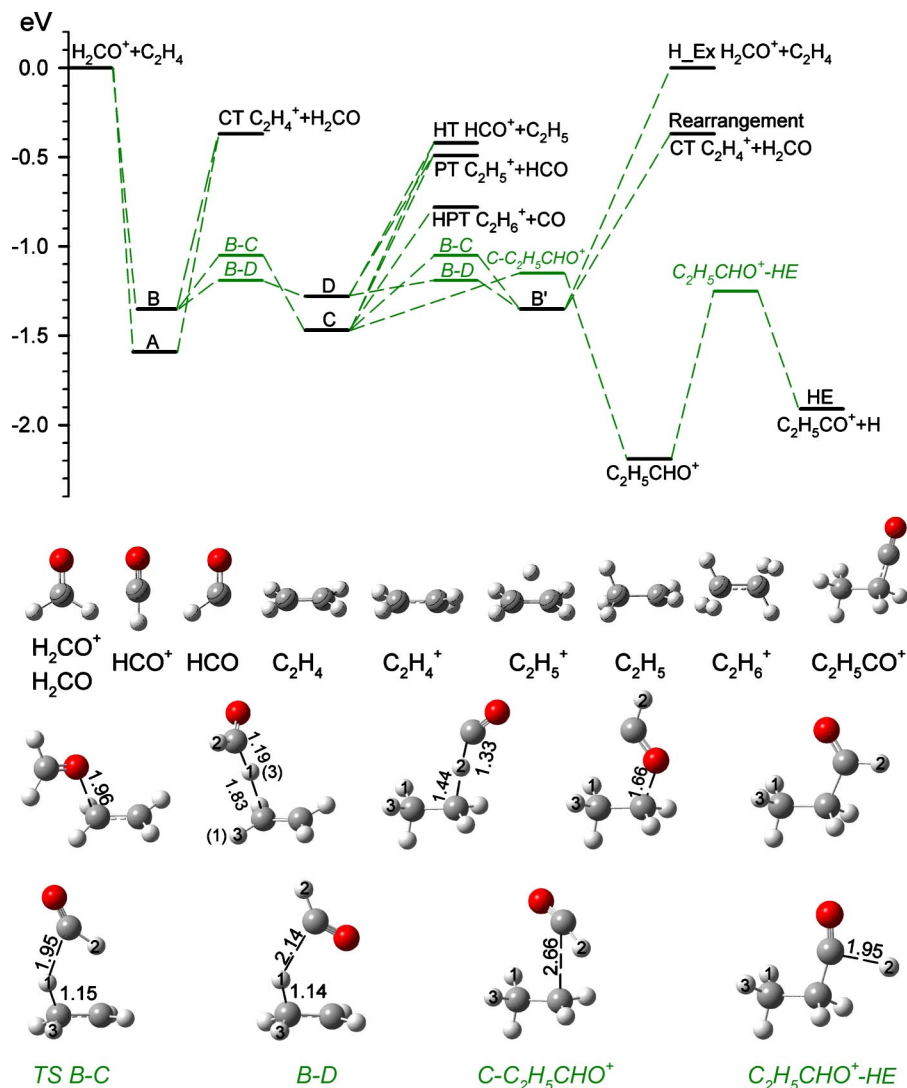


FIG. 2. Schematic reaction coordinate for $\text{H}_2\text{CO}^+ + \text{C}_2\text{D}_4$. Energies are derived from a combination of experimental and B3LYP/6-311++G** values, the latter including zero-point energies.

Four weakly bound complexes (A–D) and one covalently bound complex ($\text{C}_2\text{H}_5\text{CHO}^+$) were found. We attempted to locate transition states (TSs) connecting the complexes to each other and to reactants and products, and those found are indicated in Fig. 2. We were not able to locate the TS governing interconversion between complexes A and B. Several other covalently bound $\text{C}_3\text{H}_6\text{O}^+$ isomers (e.g., $[\text{CH}_3\text{COCH}_3]^+$, $[\text{CH}_3\text{CHCHOH}]^+$, $[\text{CH}_2\text{CH}_2\text{CHOH}]^+$, $[\text{CH}_2\text{CHCH}_2\text{OH}]^+$, and $[\text{CH}_3\text{CH}_2\text{COH}]^+$) were studied computationally by Bouma, MacLeod, and Radom,¹⁹ Bouchoux, Luna, and Tortajada,²⁰ and Hudson, McAdoo, and Traeger.²¹ These species are not included in the reaction path outlined in Fig. 2 because their formation involves either activation barriers inconsistent with the experimental energy dependence or complicated rearrangements that are inconsistent with the very short reaction time scale observed here (see below). If these additional complexes were included, they would probably contribute only to the minor HE channel. To participate in any of the major channels, complicated rearrangements would be required in both the entrance and exit channels.

Complexes A and B can be characterized as reactantlike, but are bound by 1.4–1.6 eV. Complex A has H_2CO electro-

statically bonded to one of the carbon atoms in ethene with a $\text{H}_2\text{CO}-\text{CH}_2\text{CH}_2$ distance of 1.96 Å. Natural population analysis (NBO) (Ref. 22) indicates that in complex A the charge is 72% transferred to the ethene moiety, thus this complex is productlike from the perspective of CT. Complex B has H_2CO^+ hydrogen bonded to a C atom in ethene with a H–C distance of 1.83 Å, and here, the charge is roughly equally distributed between the H_2CO and C_2H_2 moieties. Because no rearrangement is required to form these reactantlike complexes, it is unlikely that there would be activation barriers to their formation, and the large cross section observed for CT suggests that the charge transfer needed to form complex A should also be facile.

Complexes C and D are productlike, formed by hydrogen-bond and electrostatic interactions, respectively. Complex C has appropriate geometry to dissociate to HT, PT, and HPT products by single bond scission, whereas complex D connects directly only to HT and PT products. The covalently bound $\text{C}_2\text{H}_5\text{CHO}^+$ complex is the most stable of the five complexes, and is the obvious complex to mediate the H elimination (HE) channel. This complex can also lose HCO , HCO^+ , or CO generating PT, HT, or HPT products, how-

TABLE I. Experimental and calculated $\Delta_r H^\circ$ (eV) relative to reactants ($\text{H}_2\text{CO}^+ + \text{C}_2\text{H}_4$).

Reaction energetics	$\Delta_r H^\circ$ (298 K)	
	B3LYP/6-311++G** ^a	Experimental ^b
$\rightarrow \text{H}_2\text{COH}^+ + \text{C}_2\text{H}_3$	0.22	0.28
$\rightarrow \text{HCO}^+ + \text{C}_2\text{H}_5$	-0.23	-0.42
$\rightarrow \text{C}_2\text{H}_4^+ + \text{H}_2\text{CO}$	-0.54	-0.37
$\rightarrow \text{C}_2\text{H}_5^+ + \text{HCO}$	-0.52	-0.49
$\rightarrow \text{C}_2\text{H}_6^+ + \text{CO}$	-0.86	-0.78
$\rightarrow \text{C}_2\text{H}_5\text{CO}^+ + \text{H}$	-1.34	-1.91
Complex A	-1.59	...
Complex B	-1.35	...
Complex C	-1.47	...
Complex D	-1.28	...
$\text{C}_2\text{H}_5\text{CHO}^+$	-2.19	-2.29
TS(B-C)	-1.05	...
TS(B-D)	-1.19	...
TS(C- $\text{C}_2\text{H}_5\text{CHO}^+$)	-1.15	...
TS($\text{C}_2\text{H}_5\text{CHO}^+ - \text{HE}$)	-1.25	...

^aZero point energy calculated at B3LYP/6-311++G** was scaled by 0.9804.

^bExperimental values of $\Delta_r H^\circ$ (298 K) are taken from Refs. 14, 15, and 39.

ever, both energetics and transition state tightness suggest that HE will dominate its decay.

Figure 2 shows reaction paths suggested by the calculations. The CT channel is dynamically simple in that no rearrangement is needed and there are no barriers along the reaction coordinate. Observation of a CT cross section in excess of $\sigma_{\text{collision}}$ at higher collision energies indicates that CT must be possible at large interreactant separations, without any strong dependence on reactant orientations. CT may be complex mediated at low collision energy, but complex formation is certainly not required. The lowest energy routes found to HT and PT products are reactants \rightarrow complex B \rightarrow TS(B-C)[or TS(B-D)] \rightarrow complex C[or complex D] \rightarrow HT and/or PT products. In decay of complexes C and D, branching between PT($\text{HCO} + \text{C}_2\text{H}_5^+$) and HT($\text{HCO}^+ + \text{C}_2\text{H}_5$) will depend on both the energetics of the product charge states and also on the nature of how the charge states decouple as the products separate. Assuming that the charge state electronic coupling is strong, the branching, in absence of dynamical effects, should just be determined by the number of accessible vibronic levels belonging to the two electronic states.²³

The only low energy route found to HPT products is reactants \rightarrow complex B \rightarrow TS(B-C) \rightarrow complex C \rightarrow HPT. We also computed a pathway for the H_{Ex} channel, i.e., for H/D exchange between H_2CO^+ and C_2D_4 . Both complexes C and D are good candidates for mediating the actual H/D exchange event, which in this case requires only rotation of the methyl (i.e., CD_2H) group. To generate H_{Ex} products, the exchanged D atom must be transferred back to the HCO moiety. The H_{Ex} path is thus reactants \rightarrow complex B \rightarrow complex C or D \rightarrow complex B' \rightarrow H_{Ex} products. Complexes B and B' differ only in H/D exchange of the atoms labeled 1 and 3. When complex B' dissociates, it can generate either $\text{HDCO}^+ + \text{C}_2\text{D}_3\text{H}$ or $\text{HDCO} + \text{C}_2\text{D}_3\text{H}^+$ products, depending on which fragment gets the charge. In either case, the ionic product is mass 31, thus the H_{Ex} cross section

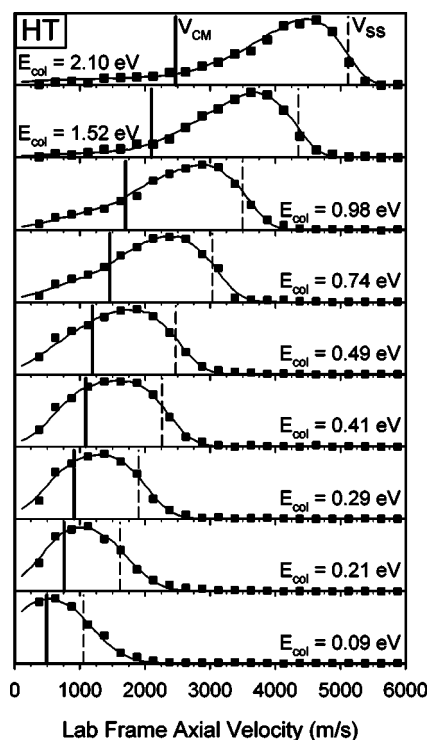


FIG. 3. Axial recoil velocity distributions for the HT channel. Solid symbols: experimental. Solid line: simulation based on the osculating complex model. Heavy vertical line: $\langle V_{\text{c.m.}} \rangle$. Dashed line: spectator stripping limit product velocity.

includes contributions from both simple H/D exchange and H/D exchange accompanying CT. Finally, the minimum energy pathway to HE products suggested by the calculations is reactants \rightarrow complex B \rightarrow TS(B-C) \rightarrow complex C \rightarrow TS(C- $\text{C}_2\text{H}_5\text{CHO}^+$) \rightarrow $\text{C}_2\text{H}_5\text{CHO}^+ \rightarrow$ TS($\text{C}_2\text{H}_5\text{CHO}^+ - \text{HE}$) \rightarrow $\text{C}_2\text{H}_5\text{CO}^+ + \text{H}$. Even though HE is the most energetically favorable channel, it accounts for less than 2% of σ_{total} , even at our lowest E_{col} .

C. Recoll velocity distributions

TOF data were collected for product ions at a series of E_{col} values and for each vibrational state. Velocity distributions for the HE channel were not analyzed because the heavy ion-light neutral kinematics are poor for extracting useful information. The lab frame v_{axial} distributions for HT, H_{Ex}, CT, PT, HPT product ions are given in Figs. 3–7, respectively. Also shown as solid vertical lines in each figure are the velocities of the c.m. frame with respect to the lab frame, $\langle V_{\text{c.m.}} \rangle$, averaged over distributions of reactant ion and target velocities. For comparison, the velocities (V_{ss}) expected from the spectator-stripping mechanism²⁴ are indicated with dashed vertical lines in Figs. 3 and 6.

Axial velocity (v_{axial}) distributions are simply the projection of the full velocity distributions on the ion guide axis. Because our experiment is axially symmetric, the lab frame v_{axial} distributions can be approximately converted to the c.m. frame simply by subtracting $\langle V_{\text{c.m.}} \rangle$. The raw lab-frame v_{axial} distributions, thus, provide useful dynamical insight. For example, if reaction is mediated by a complex with lifetime ($\tau_{\text{collision}}$) greater than its rotational period (τ_{rotation}), the

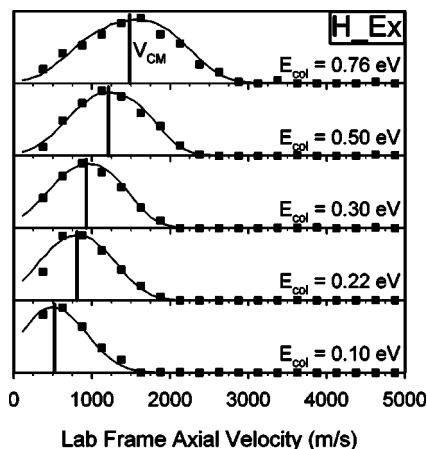


FIG. 4. Axial recoil velocity distributions for the H_Ex channel. Solid symbols: experimental. Solid line: simulation based on the osculating complex model. Heavy vertical line: $\langle V_{\text{c.m.}} \rangle$.

resulting v_{axial} distribution must be symmetric about $\langle V_{\text{c.m.}} \rangle$. Conversely, an asymmetric v_{axial} distribution is a clear sign that reaction is direct (i.e., not complex mediated) and also reveals the dominant scattering mechanism (i.e., forward vs backward scattering). Finally, some insight into the partitioning of available energy into product recoil can be inferred from the v_{axial} distribution. There are a few limitations of this technique as implemented here. Product ions that are strongly backscattered in the c.m. frame may have negative laboratory velocities. To collect such ions, the ion lens at the ion guide entrance is biased positive relative to the guide potential, reflecting these ions back toward the detector. The

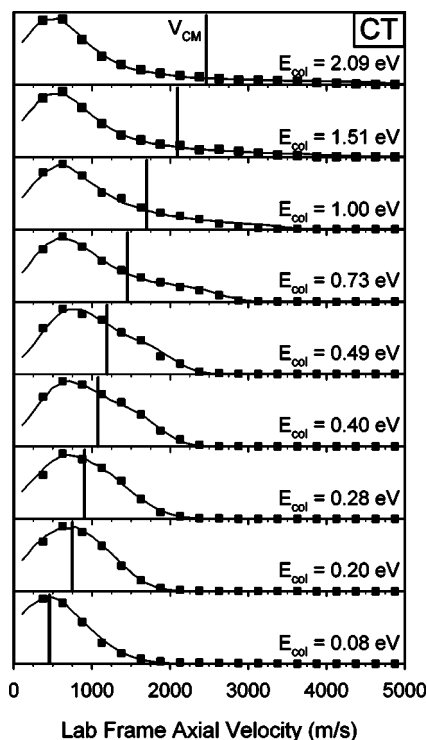


FIG. 5. Axial recoil velocity distributions for the CT channel. Solid symbols: experimental. Solid line: simulation based on the osculating complex model. Heavy vertical line: $\langle V_{\text{c.m.}} \rangle$.

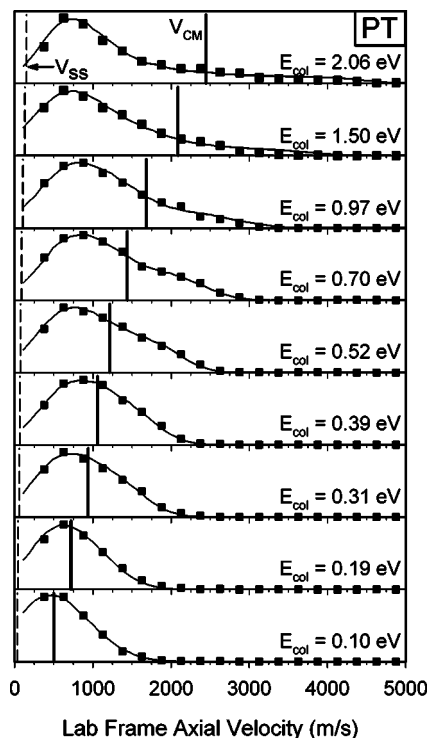


FIG. 6. Axial recoil velocity distributions for the PT channel. Solid symbols: experimental. Solid line: simulation based on the osculating complex model. Heavy vertical line: $\langle V_{\text{c.m.}} \rangle$. Dashed line: spectator stripping limit product velocity.

reflected ions appear at long flight times, corresponding to low but positive lab velocities. In addition, the slowest ions are most likely to undergo secondary reactions and to have their velocities distorted by small inhomogeneities in the surface potentials on the ion guides. Finally, these distortions in the low velocity portion of the v_{axial} distributions are exacerbated by the singular TOF-to-velocity Jacobian. The problem appears to be significant for the CT, PT, and HPT channels, as they produce the slowest product ions. In fitting the velocity distributions, data points at velocities below 450

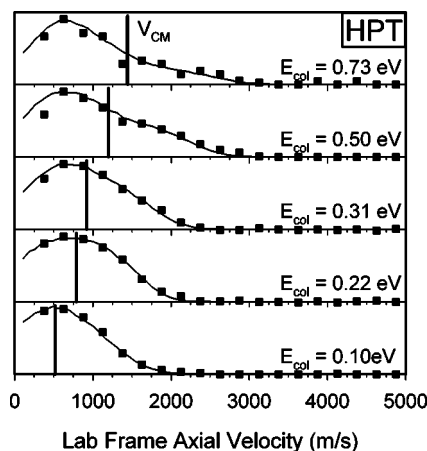


FIG. 7. Axial recoil velocity distributions for the HPT channel. Solid symbols: experimental. Solid line: simulation based on the osculating complex model. Heavy vertical line: $\langle V_{\text{c.m.}} \rangle$.

m/s, where the distortions are most problematic, are given zero weight.

At high E_{col} the v_{axial} distributions for all channels (except H_Ex) are strongly asymmetric with respect to $\langle V_{\text{c.m.}} \rangle$, indicating direct reaction mechanisms. The distributions for HT are peaked well forward of (faster than) $\langle V_{\text{c.m.}} \rangle$, while the distributions for CT, PT, and HPT are backward peaked (i.e., slower than $\langle V_{\text{c.m.}} \rangle$). Note that “forward” and “backward” are defined as product ions with axial velocities faster or slower, respectively, than $\langle V_{\text{c.m.}} \rangle$. With this definition, the sense of forward and backward are opposite for channels where the charge is transferred (PT,CT,HPT) compared to those where it is not (HT). In this system, all major channels at high E_{col} are dominated by stripping type mechanisms, i.e., by collisions at large impact parameters leading to transfer of e^- , H, H^+ , or H_2^+ , without major deflection of the collision partners. In addition, the presence of tails in the v_{axial} distributions well into the backward (HT) or forward (CT, PT, and HPT) directions suggests that small impact parameter collisions also contribute to all the major channels, leading to rebounding product ions. It is not surprising that stripping-type dynamics are dominant for the major channels—the large cross sections imply that these reactions must be possible in larger impact parameter collisions. For HPT, on the other hand, the small cross section ($\sim 0.01 \sigma_{\text{hardsphere}}$ at $E_{\text{col}} > 1$ eV) is consistent with two limiting-case mechanisms. It could be that HPT occurs only in small b collisions, or alternatively, that a broad range of impact parameters contribute, but with very low efficiency. The strongly backward peaked v_{axial} distributions show that the latter interpretation is closer to reality.

As E_{col} is reduced, the peak of the v_{axial} distributions for all product channels shifts toward $\langle V_{\text{c.m.}} \rangle$, such that by the lowest E_{col} the distributions appear forward-backward symmetric with respect to $\langle V_{\text{c.m.}} \rangle$. At the same time, however, $\langle V_{\text{c.m.}} \rangle$ decreases to only 480 m/s at the lowest E_{col} —only slightly greater than the ~ 450 m/s velocity below which we feel that our velocity measurements are unreliable. Because we have essentially no information about the slow half of the v_{axial} distributions at low E_{col} , the fact that all product channels can be fit assuming forward-backward symmetry is inconsequential. What is clear, however, is that the distributions for all channels except H_Ex become asymmetric as collision energy is raised. The shape of the distributions is consistent with a complex-mediate mechanism at low E_{col} , becoming increasingly direct with increasing E_{col} as the collision time becomes shorter.

The exception is the H_Ex channel, where the v_{axial} distributions remain forward-backward symmetric over the entire E_{col} range where $\sigma_{\text{H_Ex}}$ is large enough to allow v_{axial} measurements. This behavior suggests that the H_Ex channel requires mediation by a long-lived complex. As E_{col} is raised, rather than switching to a direct mechanism, the H_Ex channel simply disappears.

The velocity distributions for all channels were fit using the osculating complex model,²⁵ appropriate for a mechanism that transitions between complex mediate and direct with E_{col} . Fitting allows us to extract somewhat more quantitative insight from the distributions, by accounting for ex-

perimental broadening resulting from the angular and velocity distributions of both reactants. Our fitting program and procedures have been described previously.² In the osculating complex model, a short-lived collision complex is assumed to form, with rotational angular momentum (and period, τ_{rotation}) determined by the orbital angular momentum of the collision. The collision complex is assumed to decay to products with a lifetime τ_{complex} and recoil energy distribution, $P(E_{\text{recoil}})$. Here $P(E_{\text{recoil}})$ is assumed to be a Gaussian distribution parametrized in terms of the available energy (E_{avail}) in each product channel. A parameter is also included to allow the peak value and width of $P(E_{\text{recoil}})$ to decay as the complex rotates, to model the expected redistribution of energy over the course of the complex lifetime. The most important aspect of the fits, the degree of forward-backward symmetry, depends only on the ratio $\tau_{\text{collision}}/\tau_{\text{rotation}}$. To put $\tau_{\text{collision}}$ on an absolute basis, τ_{rotation} can be estimated from the moment of inertia and angular momentum of the complex, the latter estimated from the magnitude of the cross section and E_{col} . Assuming a complex like A in Fig. 2, forming with cross section at the collision limit, τ_{rotation} drops smoothly from ~ 0.9 ps at $E_{\text{col}} = 0.1$ eV to 0.35 ps at $E_{\text{col}} = 2.1$ eV. The solid curves shown in Figs. 3–7 are the fits, and the numerical results are summarized in Table II. For the H_Ex and HPT channels, simulations were only done for $E_{\text{col}} \leq 0.75$ eV because at higher E_{col} the ion intensities are too low for meaningful v_{axial} measurements.

With the exception of the H_Ex channel, $\tau_{\text{collision}}$ drops rapidly with increasing E_{col} reflecting the increasingly asymmetric v_{axial} distributions. As an indication of the collision time that might be expected in the limit of a direct mechanism, Table II also gives $\tau_{\text{fly-by}}$ taken as the time required for reactants to move a relative distance of 5 Å. For the HT channel, $\tau_{\text{collision}}$ is comparable to $\tau_{\text{fly-by}}$ at all collision energies. For CT, PT, and HPT, $\tau_{\text{collision}}$ exceeds $\tau_{\text{fly-by}}$ at low E_{col} , but becomes comparable by $E_{\text{col}} \sim 0.5$ eV. Clearly, any complexes that form are short lived. The only exception is H_Ex, where the collision time remains long (i.e., $\tau_{\text{collision}} > \tau_{\text{rotation}}$) over the entire energy range where this channel is observed. It should be noted that in the osculating complex model, the degree of forward-backward symmetry is assumed to result entirely from rotation of a collision complex. At high E_{col} where $\tau_{\text{collision}}$ is negligible, the shape of the v_{axial} distributions are probably more sensitive to the distribution of impact parameters contributing to each product channel, as discussed above.

Table II also includes estimates of the average energy partitioned into recoil $\langle E_{\text{recoil}} \rangle$ extracted from the fits. For CT, PT, and HPT, the $\langle E_{\text{recoil}} \rangle$ values extracted should be lower limits on the true values, because ions with low lab velocities (i.e., high c.m. velocities) are excluded from the fits. The tables give both $\langle E_{\text{recoil}} \rangle$ and the fraction of E_{avail} going into recoil ($\langle E_{\text{recoil}} \rangle / \langle E_{\text{avail}} \rangle$). For all channels except the H_Ex, both $\langle E_{\text{recoil}} \rangle$ and $\langle E_{\text{recoil}} \rangle / \langle E_{\text{avail}} \rangle$ increase with increasing E_{col} , consistent with faster collisions not allowing energy initially in translation to be converted to internal energy. For H_Ex, the $\langle E_{\text{recoil}} \rangle / \langle E_{\text{avail}} \rangle$ ratio decreases with increasing E_{col} , as expected for a complex-mediated mechanism. In a long-lived complex, the available energy is

TABLE II. Product ion velocity distribution fit results for $\text{H}_2\text{CO}^+ + \text{C}_2\text{D}_4$.

E_{col} (eV)	$\langle E_{\text{avail}} \rangle^a$ (eV)	$\langle E_{\text{recoil}} \rangle$ (eV)	$\langle E_{\text{recoil}} \rangle / \langle E_{\text{avail}} \rangle$ (%)	$\tau_{\text{collision}}$ (ps)	$\tau_{\text{fly-by}}^b$ (ps)
HCO^+ (HT)					
0.09	0.58	0.17	29	0.79	0.47
0.21	0.69	0.16	23	0.32	0.31
0.29	0.77	0.20	26	0.22	0.26
0.41	0.89	0.25	28	0.22	0.22
0.49	0.97	0.30	31	0.19	0.20
0.74	1.22	0.47	38	0.15	0.17
0.98	1.47	0.61	41	0.13	0.14
1.52	2.00	0.97	49	<0.10	0.12
2.10	2.58	1.48	57	<0.10	0.10
HDCO^+ (H_{Ex})					
0.10	0.16	0.07	44	2.36	0.45
0.22	0.28	0.09	32	1.94	0.30
0.30	0.36	0.10	28	1.78	0.26
0.50	0.56	0.11	20	1.54	0.20
0.76	0.82	0.18	22	0.70	0.16
C_2D_4^+ (CT)					
0.08	0.50	0.09	18	1.64	0.50
0.20	0.62	0.12	19	0.90	0.32
0.28	0.70	0.15	21	0.45	0.27
0.40	0.81	0.17	21	0.28	0.22
0.49	0.90	0.20	22	0.20	0.20
0.73	1.13	0.40	35	0.12	0.17
1.00	1.40	0.61	44	<0.10	0.14
1.51	1.92	1.05	55	<0.10	0.12
2.09	2.49	1.60	64	<0.10	0.10
$\text{C}_2\text{D}_4\text{H}^+$ (PT)					
0.10	0.65	0.07	11	2.36	0.45
0.19	0.75	0.08	11	1.29	0.33
0.31	0.86	0.15	17	0.60	0.25
0.39	0.94	0.16	17	0.55	0.23
0.52	1.06	0.25	24	0.32	0.20
0.70	1.26	0.32	25	0.22	0.17
0.97	1.53	0.48	31	0.13	0.14
1.50	2.05	0.89	43	<0.10	0.12
2.06	2.61	1.28	49	<0.10	0.10
$\text{C}_2\text{D}_4\text{H}_2^+$ (HPT)					
0.10	0.95	0.19	20	2.36	0.45
0.22	1.06	0.21	20	1.50	0.30
0.31	1.14	0.24	21	0.65	0.25
0.50	1.34	0.37	28	0.25	0.20
0.73	1.57	0.46	29	0.14	0.17

^a $\langle \cdot \rangle$ denotes mean value.

^b $\tau_{\text{fly-by}}$ defined as time for undeflected reactants to travel a relative distance of 5.0 Å.

distributed among the energetically accessible degrees of freedom, and as E_{col} increases the high frequency vibrational modes become more accessible.

Velocity distributions were also measured for reaction of vibrationally excited H_2CO^+ . These are not shown, as they are qualitatively quite similar to those for ground state reactants. The similarity reflects the fact that E_{recoil} depends mostly on E_{avail} and on the collisional energy transfer dynamics. For exoergic stripping-type reactions neither is affected much by small amounts of vibrational energy.

D. Vibrational effects

While vibration has little effect on product recoil, there are substantial effects on reactivity and product branching.

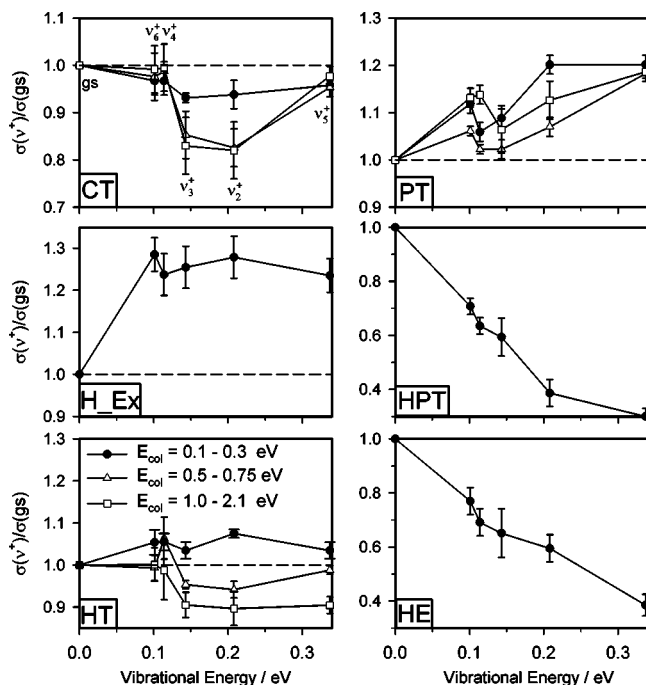


FIG. 8. Vibrational enhancement/inhibition factors vs E_{vib} , for different E_{col} ranges, for the reactions of $\text{H}_2\text{CO}^+ + \text{C}_2\text{D}_4$.

Figure 8 shows the dependence of all product channels on vibrational state. The effects are given as ratios of cross sections for reaction of a particular state $\sigma(v^+)$ to the cross section for reaction of the ground state $\sigma(\text{gs})$ plotted against E_{vib} . Each E_{vib} value corresponds to one of the six states studied, as indicated by labels in the top frame of the figure. To reduce statistical uncertainty in the ratios, data for the indicated ranges of E_{col} have been averaged. The error bars were estimated by variations between multiple data sets. Clearly, the effects of H_2CO^+ vibration are mode specific, different for different channels, and dependent on E_{col} .

IV. DISCUSSION

A. Reactions at high collision energies

The significant product channels at high E_{col} are CT, PT, HT, and HPT, and the v_{axial} distributions indicate that all channels are dominated by direct reaction mechanisms. The H_{Ex} and HE channels, which both intuition and v_{axial} distributions suggest to be complex mediated, are negligible for $E_{\text{col}} > 1$ eV.

The most obvious feature of the data at high E_{col} is that the CT cross section is $\sim 230\%$ of the collision cross section (taken as $\sigma_{\text{hardsphere}}$ for $E_{\text{col}} > 1.5$ eV). Such a large σ_{CT} implies that CT must be efficient for impact parameters (b) larger than $R_{\text{hardsphere}} (\sim 2.9 \text{ \AA})$. The maximum impact parameter where CT can occur, b_{critical} , can be estimated from the usual relation

$$\sigma_{\text{total}} = 2\pi \int_0^{\infty} P(b) b db, \quad (10)$$

where the opacity function $P(b)$ describes the reaction probability as a function of b . We use σ_{total} , rather than σ_{CT} ,

because CT occurs at long range, even in collisions that ultimately lead to other product channels (see below). $P(b)$ is a (presumably smooth) function going to zero at large b , when the collisional interaction becomes too weak to couple the $\text{H}_2\text{CO}^+ + \text{C}_2\text{D}_4$ and $\text{C}_2\text{D}_4^+ + \text{H}_2\text{CO}$ charge states. If we approximate $P(b)$ as a step function equal to 1.0 for $b < b_{\text{critical}}$ and 0 otherwise, then $\sigma_{\text{total}} = \pi b_{\text{critical}}^2$. At high E_{col} , $\sigma_{\text{total}} = 96 \text{ \AA}^2$, therefore, $b_{\text{critical}} \approx 5.5 \text{ \AA}$. Also of interest is R_{CT} —the maximum range where CT is probable. Under the assumption that $P(b)$ has a sharp cutoff at b_{critical} , we can estimate R_{CT} by simply calculating how much a trajectory at b_{critical} is deflected by the attractive long-range potential. From a classical trajectory calculated for $b = b_{\text{critical}}$, $E_{\text{col}} = 2.1 \text{ eV}$, and the appropriate ion-induced dipole potential, we find that the inward deflection is only $\sim 0.05 \text{ \AA}$, i.e., R_{CT} is $\sim 5.45 \text{ \AA}$ corresponding to $\sim 1.9R_{\text{hardsphere}}$. Because an approximate $P(b)$ was used in these estimates, they are only effective values of b_{critical} and R_{CT} .

Several factors are generally considered to be important in determining the efficiency of long-range CT.²⁶ Long range electron transfer is essentially an electronic transition, wherein the orbitals involved happen to be on different molecules. Therefore, CT probability should reflect the Franck-Condon factors connecting the initial state with accessible final states. This aspect of the mechanism is elaborated below, in the context of vibrational effects on CT. The second factor is that long-range CT should be most efficient for product states that are near resonant with the reactant state. This requirement stems from the weakness of intermolecular forces at large separations. For example, at R_{CT} the ion-induced dipole potential for $\text{H}_2\text{CO}^+ - \text{C}_2\text{D}_4$ has a value of only $\sim -0.033 \text{ eV}$ —less than 2% of E_{col} . If the potential is too weak to allow significant translational internal energy interconversion, then the CT exoergicity must be accommodated as product internal energy.

If ($T \rightarrow E_{\text{internal}}$) interconversion were truly weak, then the product ion velocity would be close to that of the neutral reactant—in this case corresponding to $v_{\text{axial}} \approx 0$ in the lab frame. Figure 5 shows that for high E_{col} , the v_{axial} distributions peak at low velocities, however, the peak is near 500 m/s in the lab frame. Taking $E_{\text{col}} = 2.1 \text{ eV}$, for example, 500 m/s corresponds to $E_{\text{recoil}} \approx 1.3 \text{ eV}$, i.e., the most probable $T \rightarrow E_{\text{internal}}$ conversion is $\sim 0.8 \text{ eV}$ of the initial 2.1 eV E_{col} . Given the weakness of the potential at long range, such efficient $T \rightarrow E_{\text{internal}}$ conversion is surprising. We observed a similar degree of $T \rightarrow E_{\text{internal}}$ conversion in a previous study¹⁸ of long-range CT in collisions of H_2CO^+ with ND_3 , but in that case substantial $T \rightarrow E_{\text{rotation}}$ conversion could be attributed to the angle-dependent ion-dipole potential that applies to both reactant and product charge states. In the present system, the C_2D_4 reactant is nonpolar, and one would expect the ion-quadrupole interaction to be insufficient to cause substantial $T \rightarrow E_{\text{rotation}}$ conversion. We believe that the explanation is that CT occurs at long range during reactant approach, such that a substantial fraction of the trajectory occurs in the $\text{C}_2\text{D}_4^+ + \text{H}_2\text{CO}$ charge state, where the neutral is polar. To test this idea, we ran a few direct dynamics trajectories at $b = 4.0\text{--}5.0 \text{ \AA}$ and $E_{\text{col}} = 2.1 \text{ eV}$, with forces calculated at the MP2/6-31G* level. Ideally, we would calculate

charge transfer trajectories for $\text{H}_2\text{CO}^+ + \text{C}_2\text{D}_4$ however, electronic structure methods suitable for use in trajectory studies are not applicable to nonadiabatic systems. To approximate the effects that might occur in the $\text{H}_2\text{CO} + \text{C}_2\text{D}_4^+$ charge state, we integrated trajectories for $\text{H}_2\text{CO} + \text{N}_2\text{H}_4^+$. This system is geometrically and kinematically nearly identical to $\text{H}_2\text{CO} + \text{C}_2\text{D}_4^+$, but the ionization energy difference (2.7 eV) is large enough that nonadiabatic effects can safely be ignored for the large impact parameter collisions of interest. Depending on the initial orientation of the reactants, we find between 0.6 and 0.8 eV of $T \rightarrow E_{\text{rotation}}$ conversion in the trajectories, mostly appearing as tumbling motion of H_2CO , as expected. This calculated rotational excitation is in reasonable agreement with the observed 0.8 eV inelasticity, suggesting that $T \rightarrow E_{\text{rotation}}$ conversion is responsible.

There are at least a couple of counterexamples indicating that $T \rightarrow E_{\text{rotation}}$ conversion can be inefficient in long-range collisions, even when one reactant has a large dipole moment. Glenwinkel-Meyer and Ottinger²⁷ studied chemiluminescence following CT of several atomic ions with HCl and found little rotational excitation. Similarly, Dressler *et al.*²⁸ looked at luminescence produced in charge transfer of several atomic ions with H_2O , and found H_2O^+ to be rotationally cold. There are several differences between these H_2O and HCl systems and our $\text{H}_2\text{CO}^+ + \text{C}_2\text{D}_4$ and ND_3 systems that account for the very different $T \rightarrow E_{\text{rotation}}$ behavior. Most important is that the product states in the H_2O and HCl experiments correspond to a molecular ion-atomic neutral, i.e., there is no ion-dipole potential to generate torque. In addition, the CT reactions are exoergic such that charge state mixing should be dominated by the product state. Therefore, if the charge state mixing occurs at long range, as suggested by the large CT cross sections/rate constants, little $T \rightarrow E_{\text{rotation}}$ conversion is expected, in agreement with the observations. In the $\text{H}_2\text{CO}^+ + \text{C}_2\text{D}_4$ and ND_3 systems, the product charge states have polar neutrals, so that torque is high through most of the collision trajectory, resulting in large $T \rightarrow E_{\text{rotation}}$ conversion.

Another factor that may affect $T \rightarrow E_{\text{rotation}}$ conversion efficiency is the relative time scales associated with rotational and translational motion. In our systems, the tumbling rotations driven by ion-dipole torque involve heavy atom motion, and thus have relatively large moments of inertia—about ten times larger than the moments of inertia for tumbling rotation of HCl or H_2O . Because all these systems have relatively large reduced masses associated with collisional motion, the implication is that the rotation-translation time scale is better matched in our systems than in the HCl and H_2O systems. It is not clear how this mass scaling might affect $T \rightarrow E_{\text{rotation}}$ conversion over the ranges of E_{col} studied in the various experiments, and it would be interesting to examine this issue with a series of trajectory studies.

In light of this discussion, we restate the rule regarding which states are accessible in long-range CT. For long-range CT where the neutral product is polar, $T \rightarrow E_{\text{rotation}}$ conversion can be efficient, but $T \rightarrow E_{\text{vibration}}$ is not. Therefore, efficient CT at long range requires that there be product vibrational states that are near resonant with the reactant vibrational state and with substantial Franck-Condon factors.

Both the large ground state CT cross section and the vibrational state dependence will be explained on this basis below. Before going on to the other high E_{col} product channels, we should emphasize that the v_{axial} results (Fig. 5) indicate that CT takes place for collisions at a wide range of impact parameters. The strong backward peak results from long-range CT, but the tail extending well into the forward direction indicates that CT also occurs in low b , repulsive collisions, where the product ion rebounds forward.

At high E_{col} the HT, PT, and HPT reactions are also direct and dominated by collisions at large impact parameters, as shown by the strongly forward (for HT) or backward (for PT and HPT) peaked velocity distributions. Also like CT, tails in the v_{axial} distributions indicate that HT, PT, and HPT occur at smaller impact parameters as well, leading to rebounding products. Unlike CT, however, these reactions involve atom transfer and presumably cannot occur at separations significantly larger than $R_{\text{hard sphere}} (\sim 2.9 \text{ \AA})$. Thus, while all channels at high E_{col} are dominated by large impact parameter collisions, HT, PT, and HPT are only able to compete with CT for $b < R_{\text{hard sphere}}$. For this range of b , however, the atom transfer reactions are quite efficient. The $\sigma_{\text{reaction}}/\sigma_{\text{collision}}$ ratios for HT, PT, and HPT at high E_{col} are 22%, 27%, and 1%, respectively, i.e., these reactions together account for 50% of the collisions at $b < R_{\text{hard sphere}}$. This 50% efficiency is roughly independent of E_{col} and the vibrational effects, while mode-specific, are only in the few percent range.

We propose that collision geometry is the main factor controlling the branching between CT and the three atom transfer channels. For $R_{\text{hard sphere}} < b < b_{\text{critical}}$, CT is the only possible reaction, and it occurs high efficiency. For $b < R_{\text{hard sphere}}$, CT and the atom transfer reactions are in competition, and the branching is most likely determined by the geometric requirement that atom transfer can only happen in collisions where one or more H_2CO^+ H atoms interact with one or more carbon center on C_2D_4 . Given the geometries of the reactants, the 50% branching suggests that atom transfer is quite efficient for those collisions in the right geometry.

The branching between HT, PT, and HPT is more interesting. HPT efficiency at high E_{col} is only $\sim 1\%$ and roughly E_{col} -independent, most likely reflecting the small fraction of collisions that have just the right geometry to transfer H_2^+ to the C_2D_4 reactant in the short collision time available. The branching between HT and PT depends on both E_{col} and vibrational state, and thus is clearly not simply determined by geometry. In fact, the HT and PT channels are just the two charge states of $(\text{HCO} + \text{C}_2\text{D}_4\text{H})^+$, thus the PT/HT branching must depend on how the energies and coupling strength of these charge states vary with separation and with various product vibrational coordinates that might be excited in the collision. The PT/HT ratio at $E_{\text{col}} = 2.1 \text{ eV}$ is 1.2. A ratio near 1 is consistent with the fact that the HT channel lies only 0.07 eV above the PT channel—a small fraction of the $\sim 2.5 \text{ eV}$ available energy. As the collision energy drops, the PT/HT ratio gradually increases to 1.4 at $E_{\text{col}} = 1 \text{ eV}$ and 3.1 at $E_{\text{col}} = 0.1 \text{ eV}$. Such an increase is expected as the PT-HT energy difference becomes a larger fraction of E_{avail} . In addition, lower E_{col} translates to slower product separation

(Figs. 3 and 6), which tends to result in more adiabatic behavior, i.e., increased production of the lower energy PT products. The vibrational effects on PT/HT branching will be discussed below.

An issue relevant to the PT/HT branching is the contribution of CID to the apparent HT product signal for E_{col} above the 1.09 eV dissociation energy of H_2CO^+ . Several observations suggest that this contribution is small. We have studied CID of H_2CO^+ in collisions with Ne and Xe,⁵ and the cross sections at 2.1 eV are, respectively, ~ 0.3 and 1.4 \AA^2 for Ne and Xe, the latter being non-negligible compared to σ_{HT} . On the other hand, in collisions with CD_4 (Ref. 17) or OCS (Ref. 29) where, as in the present system, CID competes with facile atom transfer channels, no CID signal is observed in the energy range of interest here. We also note that HCO^+ produced by CID is predominantly backscattered,⁵ whereas in the present system there is little backscattered signal at high E_{col} (Fig. 3). We conclude that CID accounts for a negligible fraction of the HT signal in this experiment.

B. Reactions at low collision energies

As the collision energy is reduced, σ_{CT} decreases to a shallow minimum near 0.4 eV, then increases slowly at low E_{col} . The increase is considerably slower than the increase in $\sigma_{\text{collision}}$ and in the cross sections for competing channels, however, so that both CT efficiency and branching fraction decrease substantially at low E_{col} . The main dynamical factor driving these effects is the increasing importance of the long-range attractive potential with decreasing E_{col} , specifically, the increase in the maximum impact parameter leading to capture, b_{capture} . At low energies b_{capture} becomes larger than b_{critical} , thus both σ_{CT} and σ_{total} become limited by capture rather than by the range at which long range CT can occur. As E_{col} is lowered, competition also becomes more important. At high E_{col} , where large b collisions are almost undeflected by the weak long-range potential, we have seen that collisions in the impact parameter range $R_{\text{hard sphere}} < b < b_{\text{critical}}$ lead to CT, with no competition from atom transfer collisions. At lower E_{col} , the attractive potential captures an increasing fraction of these collisions into the radial range where atom transfer is possible, increasing the branching to HT, PT, and HPT, at the expense of CT.

At high E_{col} all reactions clearly proceed by direct mechanisms, while for low E_{col} the v_{axial} distributions raise the possibility that some or all product channels are complex mediated. A change in mechanism may, therefore, be an issue in the product branching at low E_{col} . RRKM theory was used to explore the question of which complex(es) might have lifetimes long enough to mediate the various channels. Lifetimes were calculated for complexes A, B, C, D, and $\text{C}_2\text{H}_5\text{CHO}^+$ as a function of E_{col} . For each complex, all decomposition channels indicated by dashed lines in Fig. 2 were included. No barriers, in excess of the complex well depth, are expected for decay of complexes A and B to reactants and to CT products; decay of complex B' to H₂Ex products; and decay of complexes C and D to HT, PT, and HPT products. For these barrierless channels, we assumed orbiting transition states³⁰ with angular momentum ℓ corre-

sponding to the average capture collision, i.e., $\ell_{\text{collision}} = \mu v_{\text{rel}} (\sigma_{\text{capture}}/2\pi)^{1/2}$, where μ and v_{rel} are the reduced mass and relative velocity, respectively.

The two reactantlike complexes (A and B) were assumed to interconvert, such that complex A can also isomerize to complexes C and D, via TS(B–C) and TS(B–D). It turns out that this assumption has little effect on the lifetimes, but does have a major effect on the calculated product distribution, as discussed below. At low collision energies, the dominant decay channel for complexes A and B is to CT products, with smaller branching to complexes C and D. For both reactantlike complexes, the probability of decaying back to reactants is negligible, consistent with the observation that $\sigma_{\text{total}} \approx \sigma_{\text{collision}}$ at low E_{col} . Compared to complexes A and B, the productlike complexes C and D are less strongly bound, with higher vibrational frequencies and smaller moments of inertia. As a consequence, their lifetimes are too short (<100 fs) to have a significant effect on the collision time. The implication is that, if reaction is complex mediated at low E_{col} , the reactantlike complexes A and B must be responsible. The RRKM lifetimes for these complexes fall from a few picoseconds at $E_{\text{col}}=0.1$ eV to 0.4–0.8 ps by $E_{\text{col}}=0.5$ eV. Both the magnitude and trend are in reasonable agreement with the $\tau_{\text{collision}}$ values extracted from the v_{axial} fits. On the other hand, the existence of suitable complexes does not mean that the mechanism is necessarily complex mediated.

A better test is to compare the experimental and RRKM branching ratios. To calculate the branching, we assumed that the relative contribution from complexes A and B is determined by the ratio of the density of states in these complexes. This assumption would be true either if the complexes interconvert rapidly or if the formation probability is proportional to the density of states. The density of states is energy dependent, but even at low E_{col} the ratio is 49:51 for A:B, reflecting the fact that the available energy is much larger than the energy difference between the complexes. An issue in treating complex decay in this system is that the major decay channels are actually pairs of charge states (“back to reactants” vs CT products; HT vs PT products; both contributions to $\sigma_{\text{H}_\text{Ex}}$), and it is not obvious how branching between the charge states should be treated. The product charge state distributions will depend on the extent of charge delocalization in the complexes and on the decoupling of the charge states as the products separate. The decoupling depends on how the relative energies of the two charge states and the coupling matrix elements vary with separation coordinate. Population analysis indicates that ~72% of the charge has been transferred to the ethene moiety in complex A, while in complex B the charge is almost equally distributed between the moieties. As a first cut at the product branching, we assumed that charge state coupling was strong, such that the charge state branching is just determined by density-of-states factors.

The other important question in product branching is whether complexes A and B interconvert prior to decomposition. Initially, we calculated the branching assuming that A \rightleftharpoons B interconversion is slow. In this scenario, complex A decays almost exclusively to CT products at low E_{col} , but complex B also goes to CT products ~72% of the time,

because the orbiting TS leading to CT is much looser than TS(B–D) or TS(B–C). The net branching to CT products is calculated to be ~86%, in poor agreement with experiment (63% at $E_{\text{col}}=0.1$ eV). We then recalculated the branching under the assumption that A \rightleftharpoons B interconversion is rapid, allowing complex A to decay to complexes C and D (then on to other products) via TS(B–D) and TS(B–C). Under this assumption, the net branching to CT products at $E_{\text{col}}=0.1$ eV is 69%, still higher than the experimental (63%) CT branching, but not tremendously so. When the decay branching of complexes C and D is calculated, the net branching to all products at $E_{\text{col}}=0.1$ eV is CT:PT:HT:HPT:H_{Ex}:HE = 69:16:3:8:2:2, compared to the experimental ratio 63:19:6:7:4:2. The main discrepancy is that the calculated branching to HT products is too low. The discrepancy for HT can be rationalized by allowing a contribution from direct HT, in addition to the complex-mediated contribution. This suggestion is supported by the v_{axial} distributions which indicate shorter $\tau_{\text{collision}}$ at low E_{col} than the other channels.

At $E_{\text{col}}=0.2$ eV, the RRKM-estimated branching is CT:PT:HT:HPT:H_{Ex}:HE = 80:10:2:5:1:1, compared with the experimental ratio of 65:19:7:4:4:1. The agreement is significantly worsened for even this small increase in E_{col} , consistent with the v_{axial} results indicating that the transition from complex mediated to direct reaction is already well underway. For this reason, statistical branching was not calculated above $E_{\text{col}}=0.2$ eV.

The H_{Ex} cross section at low E_{col} (branching ~4% at $E_{\text{col}}=0.1$ eV) indicates that H/D exchange can occur with reasonable probability. The mechanism suggested by the calculations (Fig. 2) has the actual H/D exchange event occurring by methyl rotation in complex C or D, followed by conversion back to a reactantlike geometry (complex B') and dissociation to either of the isobaric HDCO⁺ and C₂D₃H⁺ product ions. In this context it is interesting to note that the HF reaction never involves D loss, despite complex C being along the reaction coordinate to C₂H₅CHO⁺, which then eliminates H to generate HE products. The absence of D-elimination products can be rationalized only if there is no scrambling of the H atom labeled 2 in the structures for complexes C and D and C₂H₅CHO⁺ in Fig. 2.

To summarize from the E_{col} dependence of the integral cross sections and v_{axial} distributions, the following mechanistic picture arises. The experimental velocity distributions and product branching are approximately in line with the predictions of a statistical model at $E_{\text{col}}=0.1$ eV, suggesting that mediation by the reactantlike complexes may be important in the mechanism. With increasing collision energy, reaction rapidly becomes direct. The H_{Ex} and HE channels, which require complex mediation, shut down completely. HPT also decreases dramatically with increasing E_{col} , however, a small and energy-independent cross section for direct HPT remains at high E_{col} . At high energies, all channels are direct, and the product distribution is dominated by CT and by the pair of atom transfer channels, HT and PT. CT/atom transfer branching is determined geometrically. PT/HT branching is determined by energetics.

C. Vibrational effects

1. Effects on CT

While σ_{CT} is nearly independent of collision energy, there are significant, mode-specific vibrational effects (Fig. 8). The ν_6^+ (in-plane CH_2 rock), ν_4^+ (out-of-plane bend), and ν_5^+ (asymmetric CH stretch) modes have little or no effect on CT probability at any energy. In contrast, ν_2^+ (CO stretch) and ν_3^+ (CH_2 scissors) significantly inhibit CT, with the effect becoming stronger with increasing E_{col} . The identical pattern of mode effects was observed for CT of H_2CO^+ in collisions with ND_3 ,¹⁸ thus it is reasonable to assume that the effects are independent of the neutral reactant. The largest effects occur in the high E_{col} range where CT is clearly dominated by a long-range electron hopping mechanism. As discussed above, efficient CT in a long-range mechanism is expected to require the existence of product vibrational states nearly resonant with and having good Franck-Condon overlaps with the reactant state. In this case, the exoergicity is 0.37 eV, and the question is “where does it go?” H_2CO^+ and H_2CO have similar geometries, thus the Franck-Condon principle is expected to favor long-range CT transitions that conserve the H_2CO vibrational state: $\text{H}_2\text{CO}^+(\nu^+) \rightarrow \text{H}_2\text{CO}(\nu)$. As a consequence, the H_2CO product is not expected to take up much of the CT exoergicity. In contrast, C_2D_4 goes from planar to a twisted geometry upon ionization, such that the $\text{C}=\text{C}$ stretch (ν_2^+) and torsion (ν_4^+) modes are Franck-Condon active in the photoelectron spectrum.³¹ It turns out that the CT exoergicity of 0.37 eV is nearly resonant with the $\text{C}_2\text{D}_4^+(0202)$ energy level, and production of this level is also strong in the photoelectron spectrum. The large CT cross section can, therefore, be rationalized in terms of high efficiency for transitions such as $\text{H}_2\text{CO}^+(\nu^+) + \text{C}_2\text{D}_4(0000) \rightarrow \text{H}_2\text{CO}(\nu) + \text{C}_2\text{D}_4^+(0202)$.

The inhibiting effects of $\text{H}_2\text{CO}^+ \nu_2^+$ and ν_3^+ vibrations on CT must involve degradation of either the Franck-Condon factors or resonance conditions for efficient CT. As noted previously,¹⁸ the H_2CO^+ geometry is essentially unchanged upon neutralization, however, the nature of the vibrational normal coordinates for ν_2^+ and ν_3^+ do change substantially. In particular, the relative contribution of CH_2 scissors and CO stretch motion in these two normal modes changes significantly between H_2CO and H_2CO^+ . Thus, although the CO bond length and HCH angles are essentially unchanged, ionization clearly changes the potential along the CO stretching and CH_2 scissors coordinates. We calculated approximate Franck-Condon factors for H_2CO^+ neutralization¹⁸ within the independent harmonic oscillator, normal mode approximation, using the Sharp-Rosenstock-Chen algorithm^{32,33} evaluated by the program PESCAL.^{34,35} As suggested by the changes in normal coordinates, the Franck-Condon factors are essentially unity (>0.97) for the diagonal transitions in all modes except ν_2^+ and ν_3^+ , where the Franck-Condon factors are 0.88 and 0.79, respectively. As in the ND_3 system, therefore, we attribute the vibrational inhibition from ν_2^+ and ν_3^+ excitation to diminished Franck-Condon overlaps for the energetically favorable transitions, requiring closer reactant approach before CT becomes efficient.

Recall that CT goes by a combination of mechanisms.

Impact parameters up to b_{capture} result in intimate collisions, some of which lead to CT products. Collisions for $b_{\text{capture}} < b < b_{\text{critical}}$ still lead to CT by long-range electron hopping. At high E_{col} , b_{capture} is small, and because of the b -weighted nature of the cross section [Eq. (10)], the vibrational effects are largely determined by the long-range component of the mechanism. At low E_{col} , b_{capture} grows, thus CT increasingly occurs in intimate collisions. At low E_{col} the vibrational mode dependence of CT becomes weaker, but remains qualitatively identical to that observed at high E_{col} . The implication is that the intimate-collision CT mechanism is weakly dependent on H_2CO^+ vibrational state, and that the residual vibrational mode dependence simply reflects the fraction of CT that continues to go by the long-range mechanism. If this picture is correct, then at $E_{\text{col}}=0.1$ eV, where $b_{\text{capture}} \approx b_{\text{critical}}$, the CT vibrational dependence should be much weaker than the effects shown in Fig. 8, where the results from $E_{\text{col}}=0.1-0.3$ eV are averaged. Such is the case.

2. Effects on other channels

In $\text{H}_2\text{CO}^+ + \text{ND}_3$,¹⁸ the vibrational mode effects on the atom transfer channels (PT and D-abstraction) are nearly identical to those observed for the CT channel, even though these channels are formally competing for product flux. The similarity suggested that CT during reactant approach increases the collision cross section, thereby enhancing all channels. The present system is quite different. The HT, PT, HPT, H_{Ex} , and HE channels show several different vibrational mode patterns that change with E_{col} in some cases. All are quite distinct from the pattern observed for CT. The vibrational effects, taken together with other evidence, provide insight into interchannel competition, the contribution of statistical complexes, and other dynamical issues.

3. The low E_{col} range

The discussion above raises the possibility that statistical intermediate complexes may be important at the lowest collision energies. We, therefore, begin by examining the extent to which a statistical model can account for the vibrational effects. First, however, we note that the appearance of vibrational mode (as opposed to vibrational energy) effects, indicates that the limiting step in the mechanism must be influenced by dynamics, i.e., the type of motion excited matters. This might seem inconsistent with a statistical mechanism, however, there is no reason that a mechanism cannot combine dynamical and statistical effects. For example, product branching and v_{axial} distributions might be controlled by statistical decay of a complex, but dynamical effects could still be important at an earlier stage of the mechanism, e.g., controlling complex formation. In this system, the dependence on vibrational mode is relatively weak, thus it is reasonable to see if a statistical model can account for the major effects of vibrational energy, before trying to rationalize the mode dependence.

Comparing the RRKM calculations at $E_{\text{col}}=0.1$ and 0.2 eV (above), gives a prediction for the effects from adding 0.1 eV of collision energy. To predict the effects of adding E_{vib} , we did a calculation with $E_{\text{col}}=E_{\text{vib}}=0.1$ eV, equivalent to

exciting ν_6^+ at our lowest E_{col} . In a purely statistical calculation, the difference between vibrational and collision energy is that increasing E_{col} also increases the angular momentum, and this tends to favor channels controlled by TSs with small rotational spacing, such as orbiting TSs. For decay of the reactantlike complexes A or B, both E_{col} and E_{vib} should enhance branching to CT (high energy, orbiting TS) relative to the atom-transfer channels, which require passing through the tighter, but lower energy TS(B–C) or TS(B–D). For $E_{\text{col}}=0.1$ and $E_{\text{vib}}=0$, the RRKM-predicted CT branching is 69%, in reasonable agreement with the 63% experimental CT branching. As expected, adding 0.1 eV of E_{col} or E_{vib} increases the calculated CT branching to 80% and 79%, respectively. Both values, however, are in poor agreement with the experimental branching ($\sim 65\%$ in both cases), suggesting that the CT mechanism is beginning to look non-statistical already for low E_{col} and E_{vib} . Given the dominance of long-range CT at high energies and the signature of long-range CT in the mode dependence even at low E_{col} , this breakdown of statistical behavior is not too surprising.

The atom transfer channels are formed by decay of the productlike complexes C and D, therefore it is conceivable that the branching *within this set of channels* might still be statistical, even if CT is not. Encouragingly, RRKM does qualitatively predict the effects of adding E_{col} on branching among these channels. Relative to $E_{\text{col}}=0.1$ eV, at $E_{\text{col}}=0.2$ eV the HT and HPT branching fractions are predicted to increase, PT is predicted to decrease slightly, and the HE and H_Ex branching fractions are predicted to decrease by a factor of ~ 2 . Comparison with Fig. 1 shows that the only qualitative error is that the HPT branching actually decreases with increasing E_{col} . One might argue, therefore, that the effects of E_{col} on branching within the atom transfer channels are at least approximately statistical, although the poor agreement for CT and HPT branching at $E_{\text{col}}=0.2$ eV indicates that reaction becomes direct at quite low collision energies.

RRKM fares much worse in predicting vibrational effects. Experimentally, ν_6^+ excitation (0.101 eV) results in effects quite different from those of 0.1 eV E_{col} addition, while, as might be expected, RRKM predicts that the effects should be qualitatively similar. The predicted vs experimental effects of ν_6^+ excitation on *branching fractions* are the following: PT—21% decrease vs 3% increase; HT—80% increase vs no change; HPT—5% decrease vs 40% decrease; H_Ex—37% decrease vs 10% increase; HE—27% decrease vs 30% decrease. The poor agreement indicates that vibrational effects are largely determined by dynamical factors, even at low E_{col} .

At the lowest energies, the atom transfer channels can be grouped based on similar vibrational effects. The HPT and HE channels show similar strong suppressions by vibrational excitation, and the effects are proportional to E_{vib} within experimental error, suggesting a non-mode-specific mechanism. Both these channels are also strongly suppressed by E_{col} , and it seems reasonable to attribute the suppressions from both E_{vib} and E_{col} to a common cause. These are the lowest energy channels, but both involve multiple atom transfers. We propose that increased energy shortens colli-

sion time, suppressing channels requiring multiple atom transfers, in favor of the higher energy, but simpler HT and PT channels. By analogy, we would expect that the H_Ex channel, which also requires multiple atom transfers, should also be suppressed by both E_{col} and E_{vib} . Suppression from E_{col} is observed, but E_{vib} actually enhances H_Ex. Evidently, some step in the H_Ex mechanism is sufficiently enhanced by vibrational excitation to override the expected inhibiting effect of increased energy content.

The PT, HT, and H_Ex channels are enhanced by vibrational excitation at low E_{col} , with mode dependence similar enough to suggest some mechanistic commonality between the channels. In particular, ν_6^+ (CH_2 in-plane rock) and ν_2^+ (CO stretch) excitation result in larger-than-average enhancement (*per unit energy*), while ν_5^+ (asymmetric CH stretch) excitation results in smaller-than-average enhancement. Even if these mode-dependent variations are factored out, a general enhancement from vibrational energy remains, which for PT and H_Ex is in contrast with the inhibiting effects of E_{col} at low energies. Evidently, vibration enhances these channels by some dynamical effect that depends generally on the partitioning of reactant energy between E_{col} and E_{vib} , and specifically on the nature of the motions excited.

The relationship between the vibrational motions and the reaction coordinate in polyatomic reactions is complex, but some correlations can be drawn. For example, PT, HT, and H_Ex all require transfer of one hydrogen atom from H_2CO^+ to C_2D_4 , with subsequent back transfer of a deuterium atom required to generate H_Ex products. Immediately following the hydrogen transfer step, the system looks like $(\text{HCO}-\text{C}_2\text{D}_4\text{H})^+$, with charge delocalized. (Delocalization is suggested by the electronic structures of the productlike complexes C and D, where both have charge \sim equally distributed between HCO and $\text{C}_2\text{D}_4\text{H}$ moieties.) HCO is strongly bent (119.5°) (Ref. 36), HCO^+ is linear,³⁷ while the HCO moiety in complexes C and D is intermediate 151° and 126° , respectively. From the perspective of the H_2CO^+ reactant, therefore, the hydrogen transfer reaction coordinate involves both breaking one of the CH bonds and partially straightening the nascent HCO moiety.

The observed enhancement patterns can partially be rationalized in these terms, at least for the two modes most obviously related to the reaction coordinate. The ν_6^+ (CH_2 in-plane rock) mode is clearly related to straightening the HCO bond, carrying the system toward a more productlike geometry, and ν_6^+ results in the largest per energy enhancement. The H_2CO^+ vibrational mode most obviously relating to breaking a CH bond is ν_5^+ , the asymmetric CH stretch. As this argument would predict, ν_5^+ enhances all three channels, however, the enhancement is smaller than from other modes on a per unit energy basis. In this context we note that ν_5^+ has had smaller-than-average per energy effects on every H_2CO^+ reaction studied,^{17,18,38} and several rationalizations can be imagined. This mode has the largest mismatch between the vibrational time scale (classical period, $\tau_{\text{classical}}=10$ fs) and the slow relative motion at low E_{col} (hundreds of femtoseconds, Table II). This is also the highest energy mode (0.337 eV), more than doubling the available energy at low E_{col} , and it may be that there are diminishing returns for

vibrational excitation at high excitation energies.

The origin of the rest of the vibrational mode pattern is unclear. For example, one of the largest per energy enhancements of HT and PT comes from ν_2^+ , the CO stretch, which is not obviously related to the reaction coordinate for these channels. Our inability to predict such effects is a reflection of how little is known about the factors that control polyatomic reactions.

4. The high E_{col} range

Aside from CT, only HT and PT have significant cross sections at high E_{col} , and both reactions are direct with strippinglike dynamics. We would expect that HT and PT, being the two charge states of $(\text{HCO}+\text{C}_2\text{D}_4\text{H})^+$, should be in competition, and the anticorrelated vibrational effects support this expectation. HT is inhibited by vibration at high E_{col} , while PT is enhanced. Note that in both cases, the vibrational effects are opposite to those from E_{col} . Note also that while the two channels have opposite vibrational effects, the sum of the two channels, $\Sigma(\sigma_{\text{HT}}+\sigma_{\text{PT}})$, shows a net enhancement: ν_6^+ , ν_4^+ , ν_2^+ , and ν_5^+ enhance $\Sigma(\sigma_{\text{HT}}+\sigma_{\text{PT}})$ by 7%, 7%, 2%, and 6%, respectively, whereas ν_3^+ has essentially no effect. As discussed above, the CT and PT/HT channels are also in competition, thus one might expect the mode effect patterns for CT and for $\Sigma(\sigma_{\text{HT}}+\sigma_{\text{PT}})$ to be anticorrelated. That is not the case, however, and the reason is simple. As discussed above, CT and $\Sigma(\sigma_{\text{HT}}+\sigma_{\text{PT}})$ compete only for collisions with $b < R_{\text{hardsphere}}$. For CT at high E_{col} , however, most products result from collisions with $b > R_{\text{hardsphere}}$, where competition with PT/HT is not an issue. $\Sigma(\sigma_{\text{HT}}+\sigma_{\text{PT}})$ is vibrationally enhanced, presumably via mechanisms similar to those responsible for the larger enhancements at low E_{col} , while CT depends on Franck-Condon factors.

ACKNOWLEDGMENT

This work was supported by the National Science Foundation under Grant No. CHE-0110318.

- ¹R. J. Green and S. L. Anderson, *Int. Rev. Phys. Chem.* **20**, 165 (2001).
- ²Y.-H. Chiu, H. Fu, J.-T. Huang, and S. L. Anderson, *J. Chem. Phys.* **102**, 1199 (1995).
- ³Y.-H. Chiu, H. Fu, J.-T. Huang, and S. L. Anderson, *J. Chem. Phys.* **105**, 3089 (1996).
- ⁴Y.-H. Chiu, Ph.D. thesis, State University of New York at Stony Brook, 1996.
- ⁵J. Liu, B. Van Devener, and S. L. Anderson, *J. Chem. Phys.* **116**, 5530 (2002).
- ⁶R. Spence and W. Wild, *J. Chem. Soc.* **1935**, 338.
- ⁷F. S. Dainton, K. J. Ivin, and D. A. G. Walmsley, *Trans. Faraday Soc.* **55**, 61 (1959).

- ⁸J. Liu, H.-T. Kim, and S. L. Anderson, *J. Chem. Phys.* **114**, 9797 (2001).
- ⁹D. Gerlich, *Adv. Chem. Phys.* **82**, 1 (1992).
- ¹⁰M. J. Frisch, G. W. Trucks, H. B. Schlegel *et al.*, GAUSSIAN 03, Gaussian, Inc., Pittsburgh, PA, 2003.
- ¹¹J. B. Foresman and A. Frisch, *Exploring Chemistry with Electronic Structure Methods*, 2nd ed. (Gaussian, Inc., Pittsburgh, 1993).
- ¹²L. Zhu and W. L. Hase, *A General RRKM Program(QCPE 644)* (Chemistry Department, University of Indiana Press, Bloomington, 1993).
- ¹³W. L. Hase, K. Bolton, P. de Sainte Claire *et al.*, VENUS99, A general chemical dynamics computer program, 1999.
- ¹⁴S. G. Lias, J. E. Bartmess, J. F. Liebman, J. L. Holmes, R. D. Levin, and W. G. Mallard, *J. Phys. Chem. Ref. Data* **17** (Suppl. 1), 1 (1988).
- ¹⁵S. G. Lias, in *NIST Standard Reference Database Number 69*, edited by P. J. Linstrom and W. G. Mallard (National Institute of Standards and Technology, Gaithersburg, MD, 2003) (<http://webbook.nist.gov>)
- ¹⁶V. G. Anicich, *An Index of the Literature for Bimolecular Gas Phase Cation-Molecule Reaction Kinetics* (National Aeronautics and Space Administration and Jet Propulsion Laboratory, California Institute of Technology Press, Pasadena, CA, 2003).
- ¹⁷J. Liu, B. V. Devener, and S. L. Anderson, *J. Chem. Phys.* **119**, 200 (2003).
- ¹⁸J. Liu, B. Uselman, B. V. Devener, and S. L. Anderson, *J. Phys. Chem. A* (in press).
- ¹⁹W. J. Bouma, J. K. MacLeod, and L. Radom, *J. Am. Chem. Soc.* **102**, 2246 (1980).
- ²⁰G. Bouchoux, A. Luna, and J. Tortajada, *Int. J. Mass Spectrom. Ion Processes* **167/168**, 353 (1997).
- ²¹C. E. Hudson, D. J. McAdoo, and J. C. Traeger, *J. Am. Soc. Mass Spectrom.* **13**, 1235 (2002).
- ²²E. D. Glendening, A. E. Reed, J. E. Carpenter, and F. Weinhold, NBO.
- ²³M. S. Child, *Molecular Collision Theory* (Academic, London, 1974).
- ²⁴R. D. Levine and R. B. Bernstein, *Molecular Reaction Dynamics and Chemical Reactivity* (Oxford University Press, New York, 1987).
- ²⁵G. A. Fisk, J. D. McDonald, and D. R. Herschbach, *Discuss. Faraday Soc.* **44**, 228 (1967).
- ²⁶J. B. Laudenslager, W. T. Huntress, Jr, and M. T. Bowers, *J. Chem. Phys.* **61**, 4600 (1974).
- ²⁷T. Glenewinkel-Meyer and C. Ottinger, *J. Chem. Phys.* **100**, 1148 (1994).
- ²⁸R. A. Dressler, M. J. Bastian, D. J. Levandier, and E. Murad, *Int. J. Mass Spectrom. Ion Processes* **159**, 245 (1996).
- ²⁹J. Liu, B. V. Devener, and S. L. Anderson, *J. Chem. Phys.* **117**, 8292 (2002).
- ³⁰M. T. Rodgers, K. M. Ervin, and P. B. Armentrout, *J. Chem. Phys.* **106**, 4499 (1997).
- ³¹L. Wang, J. E. Pollard, Y. T. Lee, and D. A. Shirley, *J. Chem. Phys.* **88**, 3216 (1986).
- ³²T. E. Sharp and H. M. Rosenstock, *J. Chem. Phys.* **41**, 3453 (1964).
- ³³P. Chen, in *Unimolecular and Bimolecular Ion-Molecule Reaction Dynamics*, edited by C. Y. Ng, T. Baer, and I. Powis (Wiley, New York, 1994), p. 371.
- ³⁴K. M. Ervin, T. M. Ramond, G. E. Davico, R. L. Schwartz, S. M. Casey, and W. C. Lineberger, *J. Phys. Chem. A* **105**, 10822 (2001).
- ³⁵K. M. Ervin, PESCAL, Fortran program, 2004.
- ³⁶G. Herzberg, *Molecular Spectra and Molecular Structure III. Electronic Spectra and Electronic Structure of Polyatomic Molecules* (Van Nostrand Reinhold, New York, 1966).
- ³⁷M. E. Jacox, *J. Phys. Chem. Ref. Data* **19**, 1387 (1990).
- ³⁸J. Liu and S. L. Anderson, *J. Chem. Phys.* **120**, 8528 (2004).
- ³⁹J. Malcolm W. Chase, *NIST-JANAF Thermochemical Tables*, 4th ed. (American Chemical Society and American Institute of Physics for the National Institute of Standards and Technology, Washington, D.C., 1998).